PCCP

Accepted Manuscript

ROYAL SOCIETY OF CHEMISTRY

www.rsc.org/pccp

Journal Name

ARTICLE

Controlling reactivity by remote protonation of a basic side group in a bifunctional photoacid

Received 00th January 20xx,
Accepted 00th January 20xx

DOI: 10.1039/x0xx00000x

www.rsc.org/

Julia Ditkovich, Dina Pines* and Ehud Pines*

6-Hydroxy-2-Naphthoic acid and its sulfonate derivatives belong to a family of bifunctional photoacids where the –OH group acts as a proton donor and the $–COO^-$ group acts as a proton acceptor. Upon electronic excitation, the –OH group becomes more acidic and the $–COO^-$ group turns more basic. Change in the ionization state of one functional group causes a change (switch) in the reactivity of the other functional group. Using picosecond time-resolved and steady state spectroscopy, we find clear evidence for an ultrafast reactivity switch caused by a diffusional proton transfer through the water solvent between the two functional groups with no evidence for a concerted proton transfer.

1. Introduction

The acid-base properties of molecules in the excited state have been studied primarily with mono-functional compounds. Aromatic compounds substituted with a hydroxyl-group, like phenols, pyranols and naphthols derivatives belong to a family of very useful ROH-type photoacids which increase their acidity typically by 5-10 pK_a units upon optical excitation.[1-4] Photoacids have been routinely used in studies of very fast proton transfer reactions. Properties of these molecules have been extensively explored.[2, 5-10] In recent years acid-base proton transfer from photoacid to carboxylate bases were studied by using time resolved uv-vis[11-13] and IR spectroscopy.[14-22]

The photophysical behavior of more complex bifunctional systems where several protonable/deprotonable groups exist simultaneously were investigated including quinolines[23-26] and aminonaphthols[27, 28]. When both the hydroxyl- and carboxy-groups are present as two substituents on the same aromatic molecule the mutual protonation state of the $-CO_2^-$ and O^- groups is expected to affect their basicity and the acidity. In *ortho*-hydroxycarboxylic acids intramolecular proton transfer occurs via a hydrogen bond already formed in the ground state along a 2-centered X-H···Y hydrogen-bonding complex.[29-31]Recently, we have demonstrated that the bifunctional photoacid 6-carboxy-2-naphthol photoacid undergoes self remote-protonation of the COO^- group following the dissociation of the OH group. The self-protonation reaction occurs by the proton diffusing through the water solvent and then protonating the basic side group.[32]

We have also studied the effect of the protonation state of a side group (COO^-) of on the acidity of the main reactive group of a photoacid, namely, the OH group of 6-carboxy-2-naphthol. The effect of the protonation state of the COO^- side group on the OH reactivity was found to be much greater in the excited state.

In the present work we report a complex photophysical behavior of a novel sulfonate derivative of 6-carboxy-2-naphthol (see Scheme 1). The sulfonate group makes the photoacid a stronger and more soluble photoacid than its parent molecule. Its main effect on the aromatic system is inductive and may be estimated from its Hammett sigma value. The basicity of the sulfonate group is low and when far apart from the OH group it cannot serve as an effective trap for the dissociating proton as carboxylate groups do.

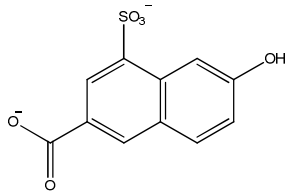

Scheme 1. 2-Naphthol-6 Carboxylate -8-Sulfonate Sodium salt (2N6C8S)

The paper is organized as follows: First, we describe the synthetic procedure and characterize the photoacidity of a novel bifunctional photoacid (2N6C8S) used in our experiments. In the following section, we describe the time-resolved measurements in H_2O and D_2O at different pHs. This allows discussing the kinetic isotope effect on the proton transfer reaction. In Section 4 we discuss how the protonation state of the carboxy-side-group effects the acidity of the OH

[a] Department of Chemistry, Ben-Gurion University of the Negev, P.O.B. 653, Beer-Sheva 84105, Israel, phone: 97286461572, email: epines@bgu.ac.il

photoacid when in the excited state. Next, we discuss the effect of a proton scavenger which we have introduced into the photoacid solutions on the self-protonation reaction of the photoacid. Finally, we substantiate our diffusion-assisted kinetic scheme for the bifunctional photoacid system which is based on the proton diffusing through the water solvent between the acid (OH) and base (COO^-) side groups.

2. Experimental

2.1 Synthetic procedure of 2-Naphthol-6-Carboxylate -8-Sulfonate Sodium salt

6-Hydroxy-2-Naphthoic acid (5g, 0.027mol) was slowly added to 9.25 ml concentrated sulfuric acid (98%) under stirring at 50^0C. Then the mixture was stirred for 3 hours while slowly increasing the temperature to 100^0C.The reaction mixture was vigorously stirred at this temperature for 1 h. Cold water was added under mechanical agitation and the resulting solution was filtrated. NaCl (2.6gr) was added to a filtrate and the resulting pinkish precipitate was filtered off and purified by crystallization from water and charcoal. 3.8 g of white product was obtained (yield 50%).
^{1}H NMR (DMSO-d8) δ 10.1 (s, OH), 8.36 (d, 1H, naphthalene), 8.32 (d, 1H, naphthalene) 8.1 (d, 1H, naphthalene), 7.9 (d, 1H, naphthalene), 7.1(dd, 1H, naphthalene).

2.2 Materials and methods

Absorption and fluorescence measurements were carried out in water. Concentrations of 4 **x** 10^{-5} M of the photoacid were typically used for the spectral measurements. The H_2O was double distilled. All spectra were acquired at room temperature (23±1^{0}C). Solutions were prepared immediately prior to spectral measurements. The steady state absorption measurements were carried out with a HP 8452A diode array spectrometer. The fluorescence spectra were taken for the same solutions with Variant Cary Eclipse Spectrometer. The transient excitation of the photoacid was done with 1 ps pulses at 355 nm using the second harmonic of the Ti-Sapphire laser operating at 710 nm. Time-correlated single-photon counting (TCSPC) measurements were carried out using a data acquisition card (SPC 130) of Becker&Hickle GmbH. The time resolution of the card was either 12 ps per channel at the 50 ns full-scale or 1.2 ps per channel at the 5 ns full-scale of the card. The kinetic decay curves were analyzed by convoluting synthetic decay profiles with the instrument response function and then searching for a best fit with the measured decay profile using Matlab software version 7.2.

3. Results

3.1 Steady-state ground state measurements

Figure 1 shows the absorption spectra of 2N6C8S as a function of the solution pH. The pH dependent absorption spectra of 6-carboxy-2-naphthol (2N6C8S) shows a behavior typical of diprotic acids with two well-separated equilibrium constants. The spectra are red-shifted compared to the absorption spectra of 2N6C8S because of influence of sulfonate group. Similar to 2N6C8S, the molecule is double protonated at low pH (HOOC-ROH) while in intermediate pH it becomes amphoteric ($^-$OOC-ROH); a basic carboxy-group with a pK_a (when protonated) of 4.17 similar to that of 2-naphthoic acid and an acidic OH group with a pK_a of 9.4 similar to that of 2-naphthol-8-sulfonate. At high pH the molecule becomes basic having the form of a double-charged anion ($^-$OOC-RO$^-$).

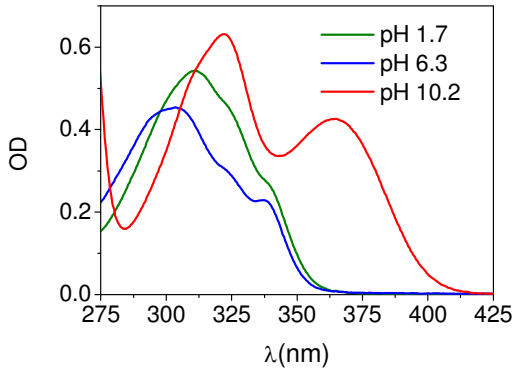

Figure 1. Absorption spectra of 2N6C8S in water at 3 representive pH values at which the monoanion (red) the neutral (red) and dianion (blue) formes of 2N6C8S dominates the absorption spectra respectively. (Absorption maxima are summarised in Table 1.)

The three ground state two-equilibrium molecular system of 2N6C8S is depicted in Scheme 2.

3.2 Steady-state excited state measurements

The complex behavior of the bifunctional photoacid system when in the electronic excited state is revealed in its steady-state fluorescence spectra taken as a function of the solution pH in water (Fig. 2)

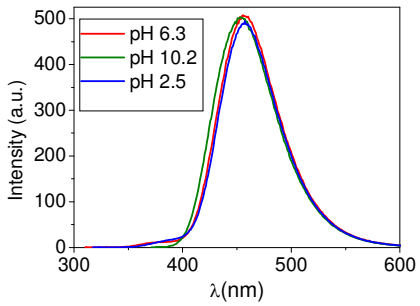

Figure 2. Steady-state fluorescence spectra of of 2N6C8S.

An isoemissive point at 400 nm appears in the fluorescence spectra and marks the existence of acid-base equilibria in the excited state of 2N6C8S at low pH. Four emitting states are expected to fluoresce from the excited 2N6C8S system: the neutral diprotic acid, HOOC-R*OH, the double ionized conjugate base of the acid, $^-$OOC-R*O$^-$ and the two monoprotoic anions $^-$OOC-R*OH and HOOC-R*O$^-$. The absorption maxima of the three ground protonation states

of2N6C8S and the fluorescence maxima of the four emitting states are listed in Table 1.

Table 1

Spectroscopic assignment of the fluorescence spectra of 2N6C8S.

	λ_{max} Fluorescence	λ_{max} Absorption
HOOC-ROH	385 nm	312.0 nm
$^-$OOC-ROH	376 nm	303.5 nm
$^-$OOC-RO$^-$	454 nm	322.0 nm
HOOC-RO$^-$	459 nm	-

Similar to what we have found for the parent 2N6C system where the fluorescence bands are well separated, we assign the 'fifth' fluorescent state to a combination fluorescence band made of the double anion fluorescence band and one of the mono-anion fluorescence bands (HOOC-R*O$^-$). Scheme 3 summarizes the four excited states of 2N6C8S and the proton transfer reactions which connect between the various protonation states. Of all the reactions only the diagonal reaction is a two stage proton-transfer reaction as marked by the colour code.

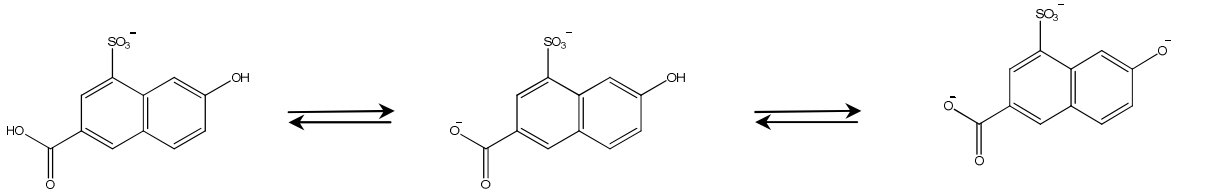

HOOC-ROH (neutral, diprotic) $^-$OOC-ROH (amphoteric) $^-$OOC-RO$^-$ (dianion, basic)

Scheme 2. Protonation states of 2N6C8S and the kinetic protonation routed connecting between them.

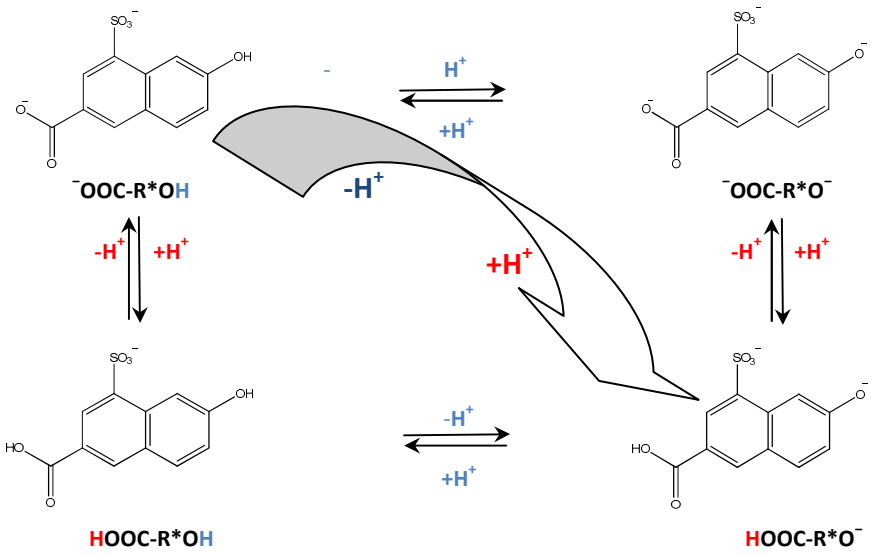

Scheme 3. The four protonation states of 2N6C8S: neutral diprotic acid, HOOC-R*OH, the double ionized conjugate base of the acid, $^-$OOC-R*O$^-$ and the two monoprotic anions $^-$OOC-R*OH and HOOC-R*O$^-$. HOOC-R*O$^-$ cannot be directly accessed from the ground electronic state and is formed in the electronic excited state of the photoacid.

We have assumed that each of the two functional groups retains its characteristic acid-base behavior as found in the reference mono-functional molecules. The 2-naphthol-8-sulfonate photoacid 2N8S (pK_a = 8.6 and pK^*_a = 1.0)[5] and 2-naphthoic acid (2NA) which is a photobase (pK_a = 4.17 and pK^*_a= 6.6) were used as the reference photoacid and photobase for elucidating the acid-base behavior of the hydroxy- and the carboxy-group in 2N6C8S respectively. We have carried out the Förster cycle spectral analysis in order to estimate the pK^*_a values for each of the protonation states in the excited state of 2N6C8S. In this analysis, the change in the proton acidity ΔpK_a upon an electronic excitation is expressed using the difference in the 0-0 transition energies of the acid and base states given by the electronic transition frequencies $\Delta\nu$ (cm^{-1}), eq (1)

$$\Delta pK_a = pK_a^* - pK_a = (0.625\ \mathrm{K}/T)(\Delta\nu/\mathrm{cm}^{-1}) \qquad (1)$$

The average spectral shifts in the maxima of the absorption and fluorescence spectra of the photoacid and photobase have been used in calculating $\Delta\nu$, T is the absolute temperature in Kelvin degrees. Table 2 summarizes the thermodynamic data extracted from the Förster cycle calculations of the pK_a* values of the photoacids.

Table 2

pKa* and pKa values of photoacids that are discussed in the text. When not indicated otherwise, pK*a values are from Förster cycle.

Photoacid	pK_a^0 (OH)	pK_a* (OH)	ΔpK_a (OH)	pK_a^0 (HO_2C)	pK_a* (HO_2C)	ΔpK_a (HO_2C)
2N6C8S (HOOC-ROH)	8.8[a]	0.5	-8.3	4.2	5.8	1.6
2N6C8S (-OOC-ROH)	9.4	1.5	-7.9	-	-	-
2N6C[32] (HOOC-ROH)	8.9[a]	1.4	-7.5	4.3	7.8	3.5
2N6C[32] (–OOC-ROH)	9.5	2.5	-7.0	-	-	-
2N8S (ROH)	9.3	1.0	-8.3	-	-	
2NA (HOOC-R)	-	-	-	4.2	6.6	2.4

[a] estimated using σ_p vs. pK_a correlation[32].

3.3 Time resolved fluorescence measurements in H_2O.

We have employed time correlated single photon counting techniques (TCSPC) in order to monitor the time behavior of the photoacid when in the electronic excited first singlet state .The dynamics of fluorescence were fitted by convoluting exponential functions which are solutions of rate equations with the instrument response function and then best-fitting the synthetic rime-resolved reaction curves with the measured one.

We have measured the time resolved fluorescence at pH 12 when both the OH moiety and the COOH side group of the photoacid were already deprotonated in the ground state (the double anionic state) and compared it to the time resolved spectra of the photoacid when excited at pH = 3.8, Fig. 3. In the latter case the neutral molecule was excited and followed by proton dissociation of the OH group to form the HOOC-R*O$^-$ anion.

The deprotonation reaction is shown in Fig. 4 where it is recorded as the decay of the acid population and the risetime of the mono-anion product. The time decay of the fluorescence approaches a $t^{-3/2}$ dependence after about 5 ns. The long-time dependence becomes apparent after correcting for the finite fluorescence lifetime of the band which was 6.6 ns (not shown). A similar asymptotic $t^{-3/2}$ power-law decay was observed for many OH photoacids[33-44] and was rationalized analytically by invoking a diffusion assisted reversible geminate recombination model.[45-47]

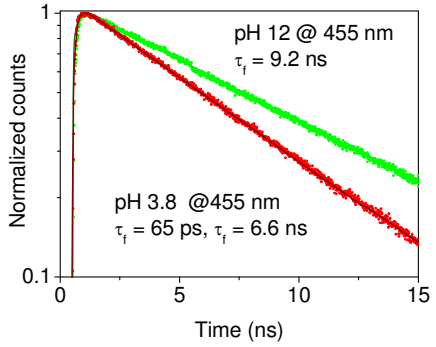

Figure 3. Time correlated single photon counting decays of the $^-$OOC-R*O$^-$ double anion, measured at 455 nm in H_2O following direct excitation at pH 12 (green dots) and of HOOC-R*O$^-$ the monoanion product following the dissociation of the neutral photoacid HOOC-R*OH at pH 3.8 (red dots). The decay time constants are 9.2 ns of the dianion and 6.6 ns of HOOC-R*O$^-$.

We have found (Fig. 5) that the dissociation rate of the OH photoacid depends on the protonation state of the COOH side group. At pH 3.8 we find that the acid population decay with exactly the same time constant as the rise of the fluorescence of the deprotonated product which was 65 ps (Figs. 4 and 5). However at pH 5.9, when the COOH side group was deprotonated in the ground state the dissociation of the OH group was slowed down to 140 ps (Fig. 5).

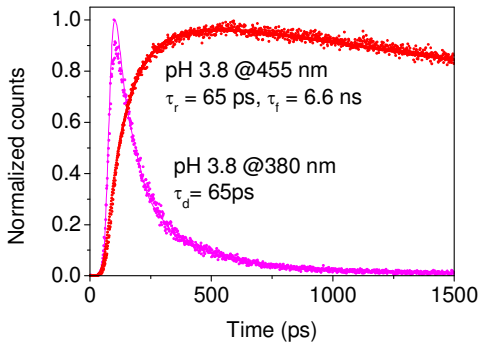

Figure 4. Time correlated single photon counting of decay of HOOC-R*OH measured at 380 nm in pH 3.8 (magenta dots, the decay time constant is 65 ps). Also shown is the rise and the decay curve of HOOC-R*O$^-$ taken from Fig. 3 and shown over an expanded time scale (red dots). Solid lines are the reconstructed synthetic decay curves.

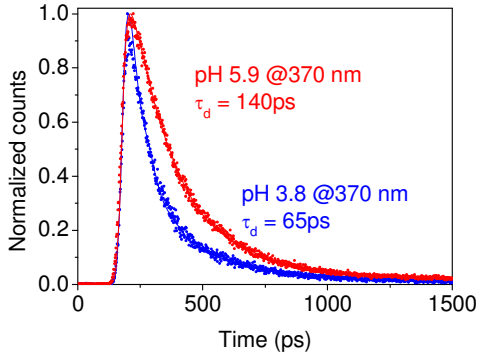

Figure 5. Time correlated single photon counting decays of HOOC-R*OH measured in H_2O at380 nm in pH 3.8 (data from Fig. 4b, red dots) and of $^-$OOC-R*OH (blue dots) measured at 370 nm in pH 5.9. Solid lines are the convolution exponential decays with the instrument response function. The decay time constants are 65 and 140 ps, respectively. Solid lines are the reconstructed synthetic decay curves.

To show that the excited state proton dissociation reaction of HOOC-R*OH is indeed reversible the time resolved dissociation of HOOC-R*OH was measured in acidic pH. Figure 6 shows the time-resolved dissociation in pH 1.3. The TCSPC data were multiplied by exp(τ_f/t) to correct for the finite fluorescence lifetime which was the excited state lifetime of the HOOC-R*O$^-$mono-anion. With increasing bulk proton concentration an equilibrium plateau developed (Fig.6). From this data the value of the excited state equilibrium constant as calculated by the Förster cycle could have been verified according to

$$K_{eq} = [H^+][RO^{*-}]_{eq}/[R^*OH]_{eq} \quad (2)$$

The calculation yielded pK^*_a = 0.5.The reversibility of the proton transfer reaction which was observed in solution pHs where the carboxy-group was fully protonated in the ground state (pH < 3.0) in not apparent when the reaction was monitored in neutral pHs such as in pH= 5.9 (Fig. 5).

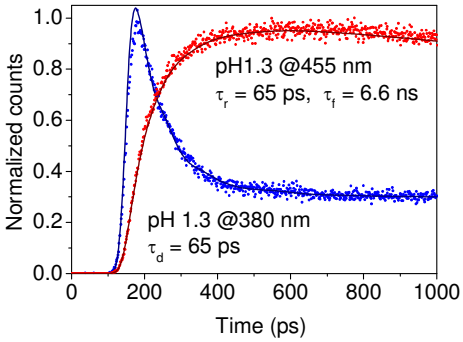

Figure 6. Time correlated single photon counting decays of HOOC-R*OH measured at 355 nm in acidic pH's, pH = 1.30. The TCSPC data were multiplied by exp(τ_f/t) to correct for the finite fluorescence lifetime which was the excited state lifetime of the HOOC-R*O$^-$ monoanion. Solid lines are the reconstructed synthetic decay curves.

A closer inspection of the decay of the acid population and the rise of the population of its conjugate base (Fig. 7) shows that the decay of the acid population and the rise of the conjugate base population are well described by a single, identical, exponent (140 ps). Unlike the situation pertaining to pH 3.8, no indication of appreciable reversible geminate recombination process was found although in this case the anion was charged. Inspection of the fluorescence decay of the product anion revealed two decay components with about ¾ of the anion population decaying with a lifetime of 6.6 ns similar to the anion lifetime found at much lower pH where the fluorescence decay was entirely of the HOOC-R*O$^-$ monoanion. Only about ¼ of the anion population decayed with the fluorescence lifetime characterizing the immediate dissociation product namely, $^-$OOC-R*O$^-$ (9.2 ns). These observations are accounted for using the reversible geminate recombination model.

At pH 3.8, the carboxylate group is protonated and so may not serve as a proton trap and compete for the proton with the -O$^-$ group. At pH 5.9, the carboxylate group is unprotonated and is free to react as a strong base with the geminate proton. In this case the carboxylate group acts as a proton scavenger effectively reducing the probability of the proton recombining back with the -O$^-$ group. These observations strongly imply, that protons generated under the above reaction conditions dominantly recombine geminately and irreversibly with the -COO$^-$ group rather than recombining reversibly with the -O$^-$ group.

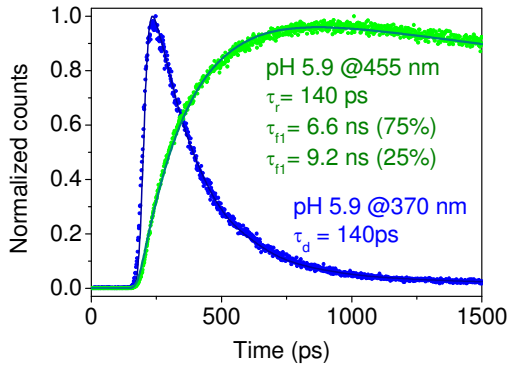

Figure 7. Time correlated single photon counting measurement in pH 5.9 of $^{-}$OOC-R*OH dissociation, measured at 370 nm) and of the product of the initiated proton dissociation reaction measured at455 nm. Solid lines are the reconstructed synthetic decay curves. The decay of $^{-}$OOC-R*OH is monoexponential with time constant of 140 ps. The signal at 455 nm rises with 140 ps time constant and decays with two decaying components, 6.6 ns (75%) and 9.2 ns (25%).

3.3. Time resolved fluorescence measurements in D_2O.

In Fig. 8a the time resolved fluorescence in pD 12.0, when both the OD moiety and the COOD side group of the photoacid were already deprotonated in the ground state, is compared to the time resolved spectra of the photoacid when excited in pD = 2.4. In this pD the neutral molecule was excited and then followed by proton dissociation of the OD group to form the DOOC-R*O^{-} anion. The deprotonation reaction is shown in Fig. 8b as the decay of the acid population and the rise-time of the mono-anion product.

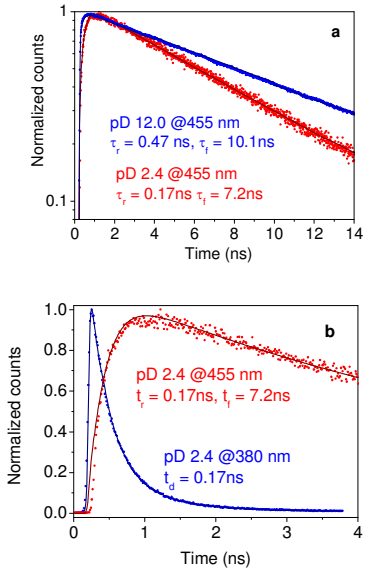

Figure 8. (a) Time correlated single photon counting decays of $^{-}$OOC-R*O^{-} measured at 455 nm in H_2O following direct excitation in pD 12.0 (blue dots) and of DOOC-R*O^{-} the monoanion product following the dissociation of the neutral photoacid HOOC-R*OH in pH 2.4 (red dots). The decay time constants are 10.1 ns of the dianion and 7.2 ns of DOOC-R*O^{-}. (b) Time correlated single photon counting of decay of HOOC-R*OD measured at 380 nm in pD 2.4 (red dots, the decay time constant is 0.17 ns). The complimentary rise and decay curve of DOOC-R*O^{-} was taken from Fig. 8a and is shown over an expanded time scale (blue dots). Solid lines are the reconstructed synthetic decay curves.

Similar to measurements in H_2O we found (Fig. 9a) that the dissociation rate of the OD photoacid depends on the protonation state of the COOD side group. In pD 2.4 we found that the acid population decays with exactly the same time constant as the rise of the fluorescence of the deprotonated product which was 0.17 ns. However in pD 6.6, when the COOD side group was deprotonated in the ground state the dissociation of the OD group was slowed down to 0.47 ns (Fig. 9a). The non-exponential long-time fluorescence tail shown in Figure 9b is the "finger print" of a diffusion assisted reversible germinal recombination process, which reforms the DOOC-R*OD form without quenching it back to the ground state.[33, 34, 45]

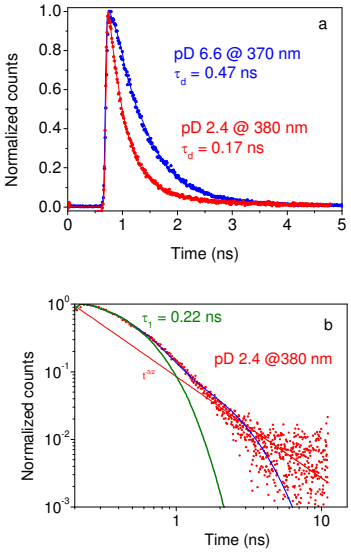

Figure 9. (a) Time correlated single photon counting decays of DOOC-R*OD measured in D_2O at 380 nm in pH 2.4 (data from Fig. 8b, red dots) and of $^{-}$OOC-R*OD (blue dots) measured at 370 nm in pH 6.6. Solid lines are the reconstructed synthetic decay curves. The decay time constants are 0.17 ns and 0.47 ns, respectively. (b) Log-log plot of the decay of the HOOC-R*OD shown in Figure 9a after the kinetic data was multiplied by exp(τ_f/t) to correct for the finite fluorescence lifetime of 7.2 ns of the DOOC-R*O^{-} mono-anion. The best monoexponential fit (green curve) and biexponential fit (blue curve) fail to reproduce the experimental data which is nicely fitted at long times by using an asymptote line , having a $t^{-3/2}$ dependence over time, of the diffusion model for a reversible geminate recombination reaction occurring at the OH group.

The decay of the acid population and the rise of the population of its conjugate base in neutral pDs (pD = 6.6) are well described by a single (97%), identical, exponent (0.47 ns). No indication of appreciable reversible geminate recombination process was found (see Fig. 10) although in this case the anion was triply charged. However, inspection of the fluorescence decay of the product anion revealed two decay components with 0.63 of the anion population decaying with a lifetime of 7.2 ns ns similar to the anion lifetime found at much lower pD's where the fluorescence decay is entirely of the DOOC-R*O^{-} monoanion. Only about 33% of the anion population decayed with the lifetime characterizing $^{-}$OOC-R*O^{-} (10.1 ns), the decay of the proton dissociation product,

which imply that the deuteron mostly recombines in neutral pDs with the COO^- group rather than with the O^- group.

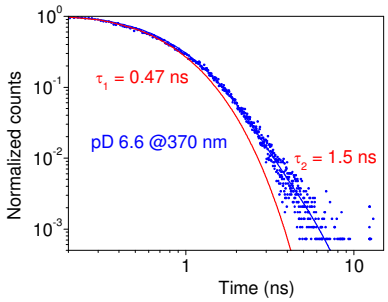

Figure 10. Log-log plot of the decay of the decays of the monoanion $^-$OOC-R*OD taken at pD 6.6 and measured at 370 nm. A monoexponential decay fits the data reasonably well up to 1 ns (red curve) and a biexponential fit (blue curve) reproduces the data very well up to 7 ns. This indicates that the extent of the back proton (deuteron)-recombination reaction to the O^- group is small under the specified reaction conditions (see detailed discussion on page 5).

4.1. Remote protonation affecting ground and excited state acidities of ROH photoacids

The free-energy levels of the various protonation states of bifunctional photoacids may be drawn using a double Förster cycle diagram where in the left side of the diagram the side group and the main functional group (the functional group responsible for photoacidity) are both protonated in the ground state and in the right side of the diagram only the main functional group is protonated in the ground state. Protonation of the $-COO^-$ side group increases the acidity of the ground state photoacid (the OH group) by about 0.6 pK_a units while in the excited state the protonation of the COO^- group increases the photoacidity of the OH group by about 1.0 pK_a units making it a strong photoacid, Scheme 3.

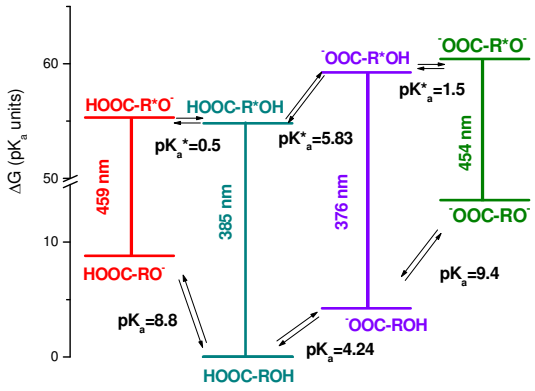

Scheme 3. The free-energy levels of the various protonation states of 2N6C8S.

4.2 Remote-protonation of the COO^- group by geminate proton recombination.

Self-protonation of the naphthalene ring following excited state proton dissociation was demonstrated and kinetically analyzed for 1-naphthol[37-39]. In this case, two competing proton recombination reactions were observed. The first one, a reversible proton recombination to the oxygen atom[33, 34, 45] and the second, irreversible proton binding to the aromatic ring, which results in quenching the molecule back to the ground state.[37-39, 48] Pines et al.[39] developed a kinetic model, which, by means of steady-state measurement combined with simple kinetic arguments, allowed a full kinetic analysis of the two coupled geminate-recombination reaction.

A similar situation prevails in the excited state proton dissociation of 2N6C8S. There, the proton may reversibly back-recombine to the O^- group or irreversibly recombine with the COO^- side group which is a strong base in the excited state (Scheme 3). Unlike the 1-naphthol case, the irreversible protonation of the side group does not quench the molecule but transfer the molecule to a different protonation state in the excited-state. Here we follow the kinetic treatment of Pines et al.[39] for the 1-naphthol/naphtholate system and apply it for elucidating the kinetic details of the proton geminate recombination reaction to the carboxy-side-group. As with 1-naphthol, the reaction is initiated in the excited state by the reversible proton dissociation of the OH group of the photoacid.

Three steady-state rate constants (see Scheme 4 and Scheme 5) are needed to characterize the reactive system of the proton-anion pair: k_s is the rate constant for the proton escaping recombination by diffusing away from the anion, k_r is the rate constant for the proton geminate recombination back to the O^- group and k_p is the rate constant for the proton geminate recombination to the COO^- side-group. ϕ_p, the quantum yield for the irreversible geminate protonation of the COO^- side-group is given by

$$\phi_p = \frac{k_p}{k_s + k_p} \qquad (3)$$

ϕ_s, the ultimate escape probability of the ion pair to form the free dianion and H^+ ions, is given by

$$\phi_s = 1 - \phi_p = \frac{k_s}{k_s + k_p} \qquad (4)$$

which satisfied the mass balance of $\phi_p + \phi_s = 1$. Rearranging we get

$$\frac{k_s}{k_p} = \frac{\phi_s}{\phi_p}; \quad k_p = \frac{\phi_p}{\phi_s} k_s \qquad (5)$$

where k_s, the diffusion controlled rate constant which separates the ion pair. k_s, is given by:

$$k_S = \frac{3DR_D}{r_0^3}\left[\exp\left(\frac{R_D}{r_0}\right) - 1\right]^{-1} \qquad (6)$$

where D is the relative diffusion coefficient between the ion pair, a is their contact radius, which also define the radius of

the reactive complex, and R_D is the Debye length which scales the coulomb interaction between the ion-pair

$$R_D = \frac{|Z_1 Z_2| e^2}{\varepsilon k_B T} \qquad (7)$$

Here, Z_1 and Z_2 are the charge numbers of the two ions, e is the electron charge, ε is the static dielectric constant of the solvent and k_BT is the Boltzmann factor. For the $^-$OOC-R*O$^-$ - H^+ pair, we use a = 5.5 Å, $D = 10^{-4}$ cm^2 s^{-1}and R_D = 21.3 x10^{-8}cm in water at 298 K.[37-39] We estimate the uncertainty in a and D to be less than 10% and 5%, respectively; this makes the total uncertainty in k_s less than 15%.

Substituting these parameters gives k_s=8.2*10^{9}s^{-1} which solving for k_p using eq (7) and the experimental value ϕ_p=75% results with k_p= 2.5 x10^{10}s^{-1}.

For the $^-$OOC-R*O$^-$- D^+ pair, we have D = 1.3 x 10^{-4} cm^2 s^{-1} which gives k_s= 8.2*10^{9}s^{-1}. Solving for k_p using eq (7) and the experimental value ϕ_p = 67% results with k_p= 1.2 x10^{10}s^{-1}. The H/D Isotope effect on the reaction rate constants is summarized in Table 3.

Table 3

Kinetic Isotope effect (KIE) for the reaction rate constants of Scheme 4 and Scheme 5.

	H_2O	D_2O	KIE
k_d (s^{-1})	7.1x10^9	2.1 x10^9	3.4
k_r (s^{-1})	7.4 x10^9	6.7 x10^9	1.1
k_p (s^{-1})	2.5 x10^{10}	1.2 x10^{10}	2.1

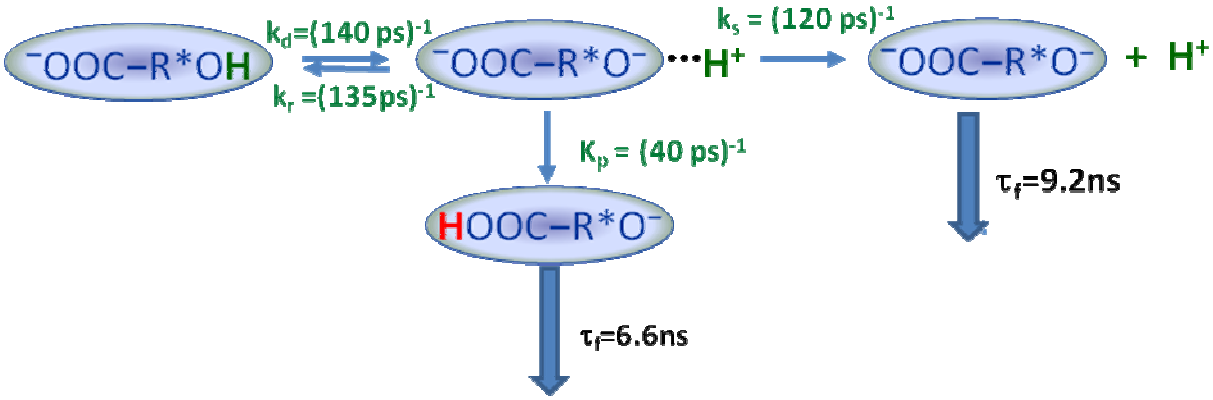

Scheme 4. Schematic representation of the kinetic system of ($^-$OOC-R*OH) which undergoes in the excited state two competing geminate-recombination reactions, one reversible and the other irreversible, designated by k_r and k_p respectively.

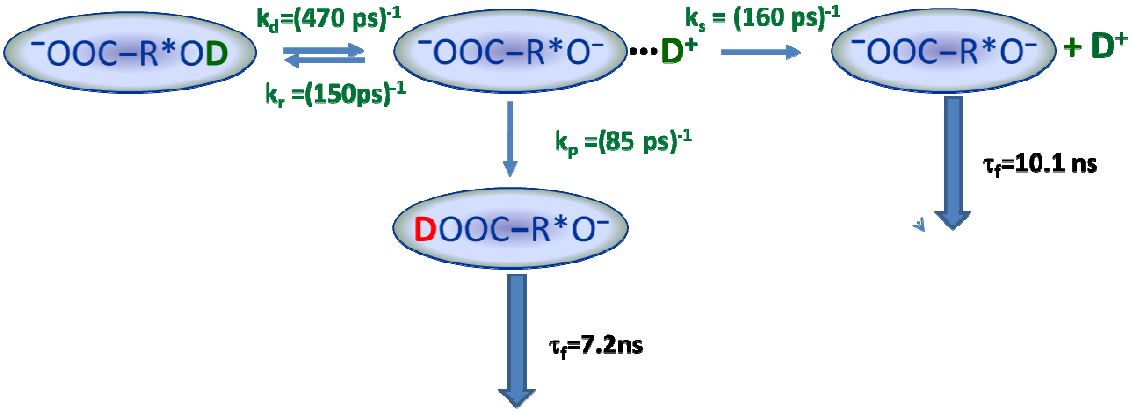

Scheme 5. Schematic representation of the kinetic system of ($^-$OOC-R*OD) which undergoes in the excited state two competing geminate-recombination reactions, one reversible and the other irreversible, designated by k_r and k_p respectively.

Journal Name

ARTICLE

The complete kinetic scheme of 2N6C8S following electronic excitation is outlined in Scheme 4 and Scheme 5. The convolutions of the numerical solutions of the kinetic Schemes 4 and 5 with the instrument response function are shown in Fig. 11.

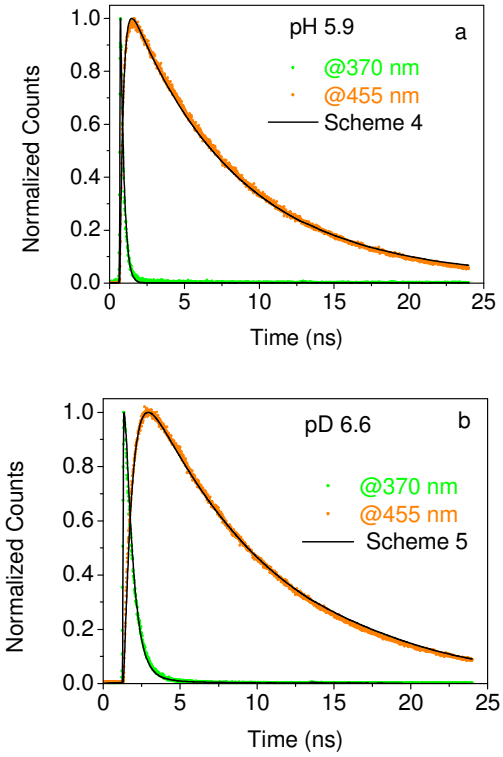

Figure 11. (a) Time correlated single photon counting of the monoanion $^{-}$OOC-R*OH decay taken in pH 5.9 and measured at370 nm (green) and the rise of the product of the geminate protonation reaction (orange) measured at455 nm. The solid lines in black are the convolution of the numerical solution of the kinetic Scheme 4 with the instrument response function. The solutions of the kinetic scheme practically overlap with the recorded experimental data. (b) Same as (a) but for D_2O. pD= 6.6 measured at370 nm for the decay of the monoanion $^{-}$OOC-R*OD and at 455 nm for the rise of the geminate deuteration product.

4.3. Verification of Remote Protonation by Geminate Proton Recombination by the Kinetic Effect of a Proton Scavenger.

A useful way for verifying the existence of a diffusion assisted geminate recombination reaction of a proton is by using proton scavengers.[36] A proton scavenger is a strong base which recombines irreversibly with the proton when it diffuses away from its geminate anion and by doing so, terminates the geminate back recombination reaction with the proton.

Time resolved fluorescence measurements of the two proton transferred products which were formed following the R*OH dissociation in pH 5.9 revealed that the relative abundance of the HOOC-R*O^{-}and $^{-}$OOC-R*O^{-} depended on the scavenger concentration (Table 4). The larger the scavenger concentration ($HCOO^{-}$) the smaller was the fraction of HOOC-R*O^{-} which was formed in the solution.

The relative amplitudes of the two proton transfer products may be directly converted to quantum yields: ϕ^{sc}_{s} of the dianion $^{-}$OOC-RO^{-} has increased and ϕ_p of the monoanion HOOC-R*O^{-} has decreased as a function of the formate anion concentration. The quantum yield information so gathered is collected in Table 4 for 0, 0.05 and 0.1 M concentration of the proton scavenger.

We attribute the observed effect of the formate anion to the scavenging reaction $HCOO^{-} + H^{+} \rightarrow$ HCOOH which is diffusion limited reaction, [36-39] k_{sc}= 5x10^{10} M^{-1}s^{-1}.

Table 4

The normalized quantum yield ϕ_s^{cs} of the dianion–OOC-R*O– in presence of a scavenger calculated from time resolved fluorescence curves as a function of the formate concentration, $c_{sc.}$

c_{sc} (M)	ϕ^{sc}_s/ϕ_s
0	1
0.05	1.55
0.1	1.8

We assume that k_{sc} depends on the ionic strength according to the Brønsted kinetic salt effect with numerical values suggested by Weller[2]

$$\log k_{sc}(I) = \log k_{sc}(0) - \frac{1.02I^{1/2}}{1+2I^{1/2}} \quad (8)$$

where I is the ionic strength of the solution which for 1:1 electrolytes is equal to the electrolyte concentration.

Following ref. [37] one may define the effective lifetime of the ion-pair τ_{sc} in the presence of a scavenger as $\tau_{sc}=1/k_{sc}(I)c_{sc}$, where $c_{sc}$is the homogeneous concentration of the scavenger. We then have using this definition

$$\frac{\phi_s^{sc}}{\phi_s} = 1 + \frac{K\pi^{1/2}\tau_{sc}^{-1/2}}{\phi_s} \quad (9)$$

where K is a constant independent of the scavenger concentration

$$K = \frac{\phi_s^{\,2} a^2 k_p}{D(\pi D)^{1/2}} \exp\left(\frac{R_D}{a}\right) \qquad (10)$$

Equation 10 predicts that ϕ^{sc}_s/ϕ_s will be linearly correlated with the square root of the scavenger concentration with a slope dependent on *K*. Figure 12 shows that this is indeed the case for the proton scavenging reactions. The slope of the line is $1.13\text{x}10^{-5}\text{s}^{1/2}$ from which we find, $K = 1.5\text{x}10^{-6}\text{s}^{1/2}$.

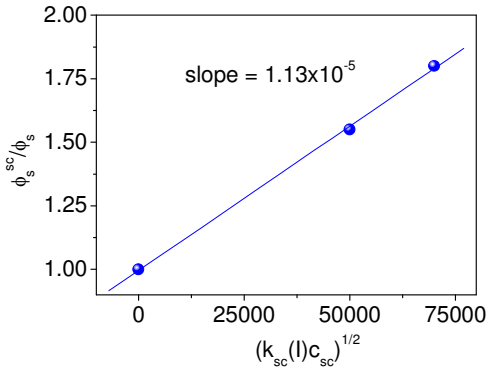

Figure 12. ϕ_s^{sc}/ϕ_s vs. $(k_{sc}(l)c_{sc})^{1/2}$ for the proton scavenging reaction of the formate anion following the proton-dissociation of the electronically excited −OOC-R*OH photoacid anion taken at pH = 5.9.

Substituting for the various parameters appearing in eq 10 we find k_p = 0.032 Å/ps which may be converted to the more common unites of a first order reaction rate using the following relation:

$$k_r(s^{-1}) = \frac{4\pi a^2 k_r}{V(a)} 10^{12}\, s^{-1} = \frac{3k_r}{a} 10^{12}\, s^{-1} \qquad (11)$$

where *V(a)* is the reaction volume having a radius of a. Using eq 11we get $k_p = 1.8\ \text{x}10^{10}\ \text{s}^{-1}$ in a good agreement with the previous calculations based on Schemes 4 and 5 and our time resolved measurements which have yielded $k_p = 2.5\ \text{x}10^{10}\ \text{s}^{-1}$. We find the isotope effect in k_d(3.4) (Table 3) to fit very well with previously measured photoacids having comparable pK^*_a values.[49] The isotope effect in k_p has two contributions since it is a tow-step process. The first process is proton diffusion through bulk water having an isotope effect in the diffusion coefficient of H^+, D_{H^+}/D_{D^+} = 1.4 at room temperature. The second contribution comes from the recombination reaction to the carboxylate anion which, judging by the relatively small isotope effect in the overall reaction (2.1), exhibits an isotope effect of a similar magnitude of about 1.5. Such a small isotope effect in the proton recombination reaction implies that the contact recombination reaction is only marginally (if at all) activated and so should be largely controlled by the solvent. This is indeed the usual case for very exothermic proton transfer reactions such as ours.[50] In this case, the proton transfer is from a strong acid (protonated bulk water are formally assigned a pK_a of -1.6) to a strong base, the carboxylate side group. The conjugate acid of the carboxylate base, the HCOO-R* side-group having according to Scheme 3 a pK^*_a of about 7. The large pK_a difference of about 8.6 units indeed implies an all-the-way down-hill contact recombination process.

The observed isotope effect in the irreversible geminate recombination reaction is thus in accord with a diffusion limited proton recombination model in the same way that the observed reaction rates of H^+ and D^+ do. It means that according to our observations and the kinetic analysis the OH moiety first dissociate to water

5. Conclusions

We conclude that bifunctional photoacids with a strong basic side group switch their excited-state reactivity according to the protonation state of the basic side group. The protonation state may be determined in the ground-state of the photoacid by the pH of the solution or may be switched in the excited state on a ps timescale by remote self-protonation. The switching of reactivity occurs by the proton dissociating from the main photoacidic group, the OH group, that then irreversibly recombines with the basic side group. In the case of the 2N6C8S photoacid, we have provided evidence that self-protonation occurs by bulk diffusion through the water solvent. This is borne out by the kinetic models that we have used which are all based on the proton diffusing through bulk water. The models also account for the observed scavenger effect and the small kinetic isotope effect. Our findings do not support a directed proton movement through several molecules-long water wires connecting between the acid group (OH) and the basic group (COO^-). Such directed movement should have resulted in a faster proton transfer reaction on the few ps time scale instead of the tens ps time scale that we observe and should have been less susceptible to the presence of proton scavengers homogeneously distributed in the solution in relatively small concentrations.

Acknowledgement

This work was supported by grant from the Israel Science Foundation 914/12 (E. P.).

References

1. T. Förster, *Die Naturwissenschaften*, 1949, **36**, 186-187.
2. A. Weller, *Prog. React. Kinet.*, 1961, **1**, 187-213.
3. L. M. Tolbert and J. E. Haubrich, *J. Am. Chem. Soc.*, 1990, **112**, 8163.
4. L. M. Tolbert and J. E. Haubricht, *J. Am. Chem. Soc.*, 1994, **116**, 10593-10600.
5. J. F. Ireland and P. A. H. Wyatt, *Adv. Phys. Org. Chem.*, 1976, **12**, 131-221.
6. L. G. Arnaut and S. J. Formosinho, *J. Photochem. Photobiol.*, 1993, **75**, 1-20.

7. L. M. Tolbert and K. M. Solntsev, *Acc. Chem. Res.*, 2002, **35**, 19 -27.
8. E. Pines, *UV-Visible spectra and photoacidity of phenols, naphthols and pyrenols* Wiley, 2003.
9. E. T. J. Nibbering, H. Fidder and E. Pines, *Annu. Rev. Phys. Chem.*, 2005, **56**, 337-367.
10. D. Pines and E. Pines, in *Physical and Chemical Aspects I-III*, eds. J. T. Hynes, J. P. Klinman, H.-H. Limbach and R. L. Schowen, Wiley-VCH: Weinheim, 2007, pp. 377-415.
11. E. Pines, B. Z. Magnes, M. J. Lang and G. R. Fleming, *Chem. Phys. Lett.*, 1997, **281**, 413-420.
12. L. Genosar, B. Cohen and D. Huppert, *J. Phys. Chem. A*, 2000, **104**, 6689 -6698.
13. B. Cohen, D. Huppert and N. Agmon, *J. Am. Chem. Soc.*, 2000, **122**, 9838 -9839.
14. M. Rini, B.-Z. Magnes, E. Pines and E. T. J. Nibbering, *Science*, 2003, **301**, 349-352.
15. M. Rini, D. Pines, B. Z. Magnes, E. Pines and E. T. J. Nibbering, *J. Chem. Phys.*, 2004, **121**, 9593-9610.
16. O. F. Mohammed, D. Pines, E. Dreyer, E. Pines and E. T. J. Nibbering, *Science*, 2005, ***310***, 83-86.
17. O. F. Mohammed, D. Pines, E. T. J. Nibbering and E. Pines, *Angew. Chem. - Intern. Ed.*, 2007, **46**, 1458-1461.
18. O. F. Mohammed, D. Pines, E. Pines and E. T. J. Nibbering, *Chem. Phys.*, 2007, **341**, 240-257.
19. M. J. Cox and H. J. Bakker, *J. Chem. Phys.*, 2008, **128**, 174501.
20. K. Adamczyk, M. Prémont-Schwarz, D. Pines, E. Pines and E. T. J. Nibbering, *Science*, 2009, **326**, 1690-1694.
21. H. J. Bakker and M. J. Cox, *J. Phys. Chem. A*, 2010, **114**, 10523-10530.
22. M. Prémont-Schwarz, T. Barak, D. Pines, E. T. J. Nibbering and E. Pines, *J. Phys. Chem. B*, 2013, **117**, 4594-4603.
23. B. K.Yoo, O. H. Kwon and D. J. Jang, *J. Phys. Chem. A*, 2004, **108**, 5932-5937.
24. H. J. Park, O. H. Kwon, C. S. Ah and D. J. Jang, *J. Phys. Chem. B*, 2005, **109**, 3938-3943.
25. O. H. Kwon, Y. S.Lee, B. K. Yoo, D. J. Jang, *Angew. Chem. Intern. Ed.*, 2006, **45**, 415-419.
26. S. Y. Park, B. Kim, Y. S. Lee, O. H. Kwon and D. J. Jang, *Photochem. Photobiol. Sci.*, 2009, **8**, 1611-1617.
27. D. W. Ellis and L. B. Rogers, *Spectrochim. Acta* 1964, **20**, 1709-1720.
28. R. Gahlaut, H. C. Joshi, N. K. Joshi, N. Pandey and S. Pant, *Spectrochim. Acta A*, 2013, **109**, 164-172.
29. W. R. Ware, P. R. Shukla, P. J. Sullivan and R. V. Bremphis, *J. Chem. Phys.*, 1971, **55**, 4048-4052.
30. H. Mishra, H. C. Joshi, H. Tripathi, S. Maheshwary, N. Sathyamurthy, M. Panda and J. Chandrasekhar, *J. Photochem. Photobiol. A* 2001, **139**, 23-36.
31. H. Mishra, H. B. Tripathi and N. Sathyamurthy, *J. Phys. Chem. A*, 2005, **109**, 2746-2754.
32. J. Ditkovich, T. Mukra, D. Pines, D. Huppert and E. Pines, *J. Phys. Chem. B*, 2015, **119**, 2690−2701.
33. E. Pines and D. Huppert, *Chem. Phys. Lett.*, 1986, **126**, 88-91.
34. E. Pines and D. Huppert, *J. Chem. Phys.*, 1986, **84**, 3576-3577.
35. A. Masad and D. Huppert, *J. Phys. Chem.*, 1992, **96**, 7324-7328.
36. S. Y. Goldberg, E. Pines and D. Huppert, *Chem. Phys. Lett.*, 1992, **192**, 77-81.
37. E. Pines and G. R. Fleming, *Chem. Phys.*, 1994, **183**, 393-402.
38. E. Pines, D. Tepper, B. Z. Magnes, D. Pines and T. Barak, *Ber. Buns. Ges. Phys. Chem. Chem. Phys.*, 1998, **102**, 504-510.
39. E. Pines, B. Z. Magnes and T. Barak, *J. Phys. Chem. A*, 2001, **105**, 9674-9680.
40. D. Pines and E. Pines, *J. Chem. Phys.*, 2001, **115**, 951-953.
41. E. Pines and D. Pines, in *Ultrafast hydrogen bonding dynamics and proton transfer processes in the condensed phase*, eds. T. Elsaesser and H. J. Bakker, Kluwer Academic Publishers, Dordrecht, 2003, pp. 155-184.
42. I. Carmeli, D. Huppert, L. M. Tolbert and J. E. Haubrich, *Chem. Phys. Lett.*, 1996, **260**, 109-114.
43. P. Leiderman, L. Genosar, N. Koifman and D. Huppert, *J. Phys. Chem. A*, 2004, **108**, 2559-2566.
44. L. Genosar, Leiderman P., Koifman N., Huppert D., *J. Phys. Chem.*, 2004, **108**, 1779-1789.
45. E. Pines, D. Huppert and N. Agmon, *J. Chem. Phys.*, 1988, **88**, 5620-5630.
46. N. Agmon, E. Pines and D. Huppert, *J. Chem. Phys.*, 1988, **88**, 5631-5638.
47. D. Huppert, E. Pines and N. Agmon, *J. Opt. Soc. Am. B*, 1990, **7**, 1545-1550.
48. K. M. Solntsev and N. Agmon, *Chem. Phys. Lett.*, 2000, **320** 262-268.
49. E. Pines, in *Isotope Effects In Chemistry and Biology*, eds. A. Kohen and H.-H. Limbach, Marcel Dekker, 2006, pp. 451-464.
50. K. Ando and J. T. Hynes, *J. Phys. Chem. B*, 1997, ***101***, 10464-104678.